Geophysical Distributions of Occultations of GPS Satellites Viewed from a Low Earth Orbiting Satellite

D.M. O'Brien and Paul Tregoning

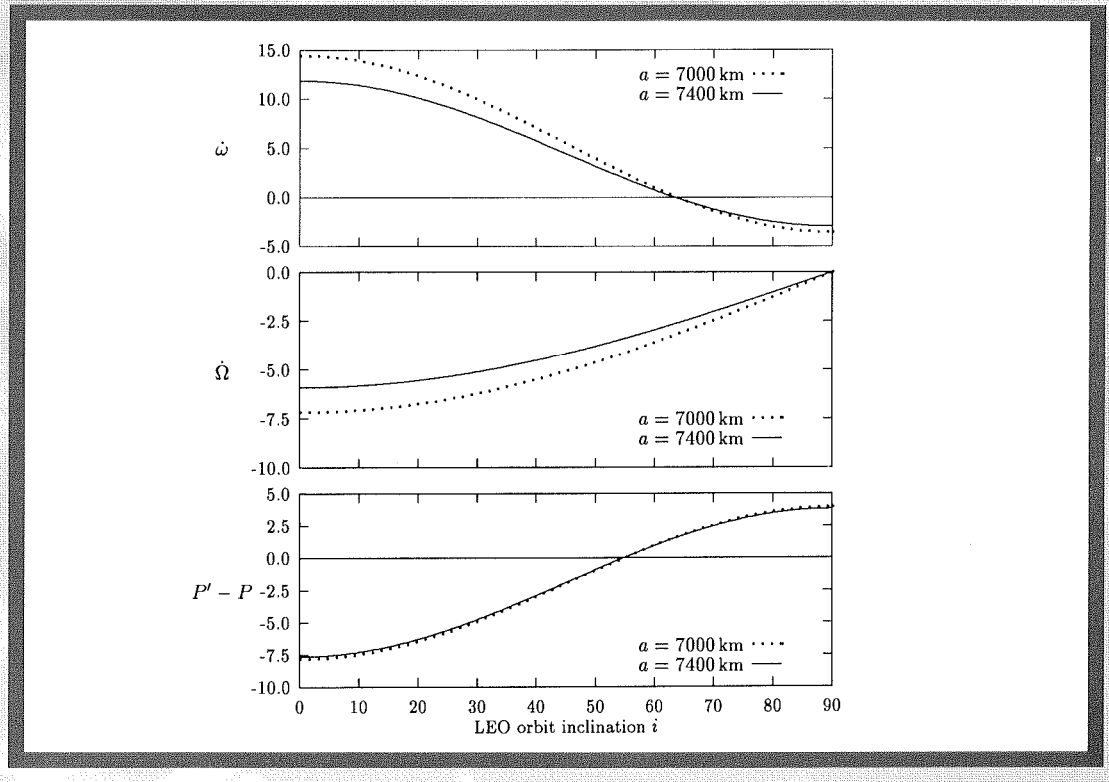

CSIRO

Atmospheric Research

CSIRO Atmospheric Research Technical Paper No. 39

Geophysical Distributions of Occultations of GPS Satellites Viewed from a Low Earth Orbiting Satellite

D.M. O'Brien and Paul Tregoning

CSIRO Atmospheric Research Technical Paper No. 39

National Library of Australia Cataloguing-in-Publication Entry

O'Brien, D. M.
Geographical distributions of occultations of GPS satellites viewed from a low earth orbiting satellite.

Bibliography.
ISBN 0 643 06345 5.
1. Global Positioning System. 2. Artificial satellites. I. Tregoning, Paul. II. CSIRO Atmospheric Research. (Series: CSIRO Atmospheric Research technical paper; no. 39).

526.982

CSIRO Atmospheric Research
PB 1, Aspendale, Victoria 3195, Australia
Ph: (+61 3) 9239 4400; Fax: (+61 3) 9239 4444
E-mail: chief@dar.csiro.au

CSIRO Atmospheric Research Technical Papers may be issued out of sequence.

Geographical distributions of occultations of GPS satellites viewed from a low earth orbiting satellite

D.M. O'Brien
CSIRO Atmospheric Research
Aspendale, Australia
and
Paul Tregoning
Research School of Earth Sciences
The Australian National University
Canberra, Australia

Abstract

The infrastructure of the Global Positioning System (GPS), with a minimum of twenty four satellites in precisely determined orbits, each transmitting on two radio frequencies of approximately 1.58 GHz and 1.23 GHz, opens new opportunities for meteorology through radio occultation. A small satellite in low earth orbit (LEO) carrying a GPS receiver will see the satellites of the GPS constellation rise and set behind the earth. From measurements of the Doppler shifts of the radio waves during occultations of the GPS satellites, it is possible to deduce the bending of the radio waves in the atmosphere of the earth, and hence determine the density profile of the atmosphere. The method is unaffected by cloud, does not involve radiometric calibration like other remote sensing methods, and provides density soundings over the entire globe.

This technical paper examines the spatial distributions of occultations for four different GPS antenna configurations on the LEO and for orbits of the LEO ranging from equatorial to polar. It is found that the most uniform spatial distribution of occultations occurs for orbits with inclinations near 60° and 120°. In addition, probability distributions are computed for the number of GPS satellites in view and the geometric dilution of precision, the latter being a measure of the accuracy with which the orbit of the LEO may be determined.

Because underflight of a GPS satellites by the LEO offer an opportunity to determine the structure of the ionsophere along radial lines from the LEO to the GPS satellite, the paper also computes the frequency of underflights and their spatial distributions.

1 Introduction

Density sounding of the atmosphere using radio occultation of GPS satellites, commonly called 'GPS meteorology', involves a low earth orbiting satellite (LEO), the constellation of GPS navigation satellites, and a network of fiducial ground stations with precise GPS receivers (Melbourne et al., 1994; Kursinski et al., 1996; Hajj et al., 1995; Eyre, 1994; Gorbunov, 1996). GPS satellites visible from the LEO along rays that do not intersect the earth's atmosphere are used in conjunction with the ground stations to determine the position and velocity of the LEO with high accuracy. The remaining GPS satellites are occulted by the earth. From precise measurements of the refraction of GPS carrier waves in the atmosphere during an occultation, the vertical profile of density in the atmosphere may be determined. This is most effective for GPS satellites occulted on or near the direction of the velocity of the LEO.

These considerations lead to the following principles guiding the selection of an orbit for GPS meteorology.

1. The orbit should ensure that sufficient GPS satellites are in view to allow precise determination of the LEO orbit. This requirement presupposes an objective measure of the effectiveness of a GPS configuration for navigation.

2. The orbit should maximize the number of occultations of GPS satellites.

3. Because meteorology is global, the orbit should ensure that the spatial distribution of occultations is uniform.

In this report, we use a numerical orbital model to track the LEO and the GPS constellation simultaneously, to determine which GPS satellites are visible from the LEO and which are occulted by the earth, and to map the spatial distribution of the occultations. We consider orbits for the LEO with inclination ranging from 0° to 180° and with right ascension of the ascending node at epoch ranging from 0° to 60°. Definitions of these angles are illustrated in figure 1. The restricted range for the latter suffices because the GPS satellites are contained in six planes equally spaced in ascending node at 30°, 90°, 150°, 210°, 270° and 330°. The eccentricity of each orbit considered for the LEO is assumed to be zero, because most earth observing satellites are in near circular orbits, and the mean anomaly at epoch is taken to be zero.

Because the forces acting on the satellites are not centrally symmetric, the orbits precess. For the GPS satellites, the rates of precession of the argument of perigee (ω) and right ascension of the ascending node (Ω) are small, but such is not the case for the LEO. In particular, the right ascension of the ascending node may precess at up to 7.5° per day, depending upon the inclination and semi-major axis of the LEO orbit. Therefore, by considering values of Ω at epoch between 0° and 60°, we are sampling different intervals of the orbital motion. These intervals overlap for low inclination orbits with rapid rates of precession, whereas for near polar orbits they are disjoint. Because the semi-major axis of the LEO orbit has only a secondary effect upon the rate of precession, we consider only one value, 7200 km, lying in the range typical of most LEOs. In practice, the semi-major axis

will be adjusted so that the LEO revisits a nominated ground station at a predetermined interval.

In addition to occultations, we determine for each orbit the number of times that the LEO underflies a GPS satellite. This information is needed to assess the practicality of probing the structure of the ionosphere along radial lines between the LEO and GPS satellites.

The visibility of GPS satellites from the LEO depends upon the location of the GPS antenna on the LEO and the field of view of the antenna, the latter defined by the maximum angle $\theta_\star$ between the antenna axis and detectable rays. We consider four bus and antenna configurations.

1. The simplest configuration assumes that the LEO is not rotating and that the GPS antenna points backwards along the track of the LEO. The field of view of the antenna is assumed to be the rearward hemisphere, specified by $\theta_\star = 90°$. This configuration is attractive because occultations fore and aft of the LEO occur in the shortest time, and hence give best horizontal localization of the density profile.

2. The simple configuration described above presents one face of the LEO to the sun during each orbit, possibly producing large temperature gradients in the bus. Therefore, it is likely that the LEO will rotate slowly about its vertical axis in order to improve the thermal regulation. In the second configuration, the antenna axis lies in the horizontal plane and rotates with the bus with a period of 10 minutes.

3. We assume in the third configuration that the GPS receiver has two antennas, inclined at 45° to the vertical and separated by 180° in azimuth. The field of view of each antenna is the hemisphere centred on the antenna axis, so $\theta_\star = 90°$. The LEO is assumed to rotate slowly about the vertical axis.

4. In the final configuration, we assume that the bus is rotating, that the antenna axis is vertical, and that the antenna field of view extends below the horizontal plane with $\theta_\star = 120°$. Such a configuration requires the antenna to be mounted upon a small pedestal above the top of the LEO. It has the advantages that the field of view is unaffected by rotation of the bus and that one antenna can be used to observe both occultations and overhead GPS satellites. However, it is unclear whether an antenna could be designed with such a wide field of view without sacrificing gain, or whether the antenna could be located on the satellite bus with an unobstructed view. Therefore, this configuration must be regarded as an attractive, but possibly impractical, idealization.

The simulations involve 26 GPS satellites, 105 possible orbits for the LEO, four antenna configurations and several indices of performance. Presentation of so much information poses the usual quandary of whether to illustrate important points with selected highlights or to include all plots in a comprehensive analysis. The compromise we have adopted shows summary information for the number of satellites in view from the LEO, the number setting behind the earth and the number of GPS underflights, while we show in greater detail the spatial distributions of occultations.

Parameter	Symbol
Semi-major axis	a
Eccentricity	e
Mean anomaly	M
Argument of perigee	ω
Inclination	i
Right ascension of the ascending node	Ω

Table 1: Keplerian orbital elements and their symbols.

2 Orbit model

2.1 Satellite positions and velocities

All orbits are assumed to be elliptical and are specified by their Keplerian elements listed in table 1. The Keplerian elements for the satellites of the GPS constellation are obtained from precise GPS orbits calculated daily by analysis of GPS data from a global network of tracking sites. The LEO orbits are assumed to precess under the influence of the non-central gravitational potential of the earth, but other forces (such as atmospheric drag, radiation and particle bombardment, and the effects of sun, moon and planets) are neglected. We write the gravitational potential of the earth in geocentric coordinates (x, y, z) in the form

$$V = \frac{K^2}{r}\left[1 + \frac{J_2}{2r^2}(1 - 3\sin^2\delta) + \frac{J_3}{2r^3}(3 - 5\sin^2\delta)\sin\delta + \ldots\right],$$

where K is the terrestrial gravitational constant, r is the distance to the spacecraft and

$$\delta = \arcsin(z/r).$$

Because the term involving J_2 dominates the higher order corrections, we discard the latter and use first order perturbations (in time) to calculate the satellite positions and velocities (Brouwer and Clemence, 1961). Omission of the higher order corrections has negligible impact on the results of this report. The non-central potential causes secular drifts of the argument of perigee and right ascension of the ascending node. The anomalistic period of the orbit, denoted P' and defined to be the time between successive passages of the perifocus, is given by

$$P' = P\left[1 + C\sqrt{1 - e^2}\left(1 - \frac{3}{2}\sin^2 i\right)\right]^{-1},$$

where P is the Keplerian period for a purely central potential,

$$P = \frac{2\pi}{K}a^{3/2},$$

and

$$C = \frac{3}{2}\frac{J_2}{a^2(1 - e^2)^2}.$$

Precession of GPS orbits	
$\dot{\omega}$	0.023°/day
$\dot{\Omega}$	-0.039°/day
$P' - P$	-0.28 ms

Table 2: Typical rates of precession of the argument of perigee and right ascension of the ascending node for GPS satellites. The inclination minimizes the difference between the anomalistic period and the period based on elliptical motion in a central potential.

The evolution of the mean anomaly, argument of perigee and right ascension of the ascending node are taken in the first order approximation to be

$$\begin{aligned} M(t) &= M_0 + \dot{M}(t - t_0), \\ \omega(t) &= \omega_0 + \dot{\omega}(t - t_0), \\ \Omega(t) &= \Omega_0 + \dot{\Omega}(t - t_0), \end{aligned}$$

where the subscript zero temporarily denotes values at epoch and the time derivatives are given by

$$\begin{aligned} \dot{M} &= \frac{2\pi}{P'}, \\ \dot{\omega} &= C\dot{M}\left(2 - \frac{5}{2}\sin^2 i\right), \\ \dot{\Omega} &= -C\dot{M}\cos i. \end{aligned}$$

The inclinations of the GPS satellite orbits have been chosen so that the anomalistic period is equal to the Keplerian period. Furthermore, the semi-major axis of the GPS orbits is so large that the rates of precession of the argument of perigee and right ascension of the ascending node are very small, as indicated by the typical values listed in table 2. In contrast, the orbit of the LEO precesses rapidly, with the rate determined principally by the inclination of the orbit. Figure 2 shows the rates of precession (in degrees per day) of the argument of perigee and the right ascension of the ascending node as a function of the inclination of the LEO orbit. Only the range $i \leq 90°$ is plotted, because $\dot{\omega}$ is symmetric about 90° while $\dot{\Omega}$ is antisymmetric. Also shown in figure 2 is the difference (in seconds) between the anomalistic period P' and the Keplerian period P. Each panel of the figure has curves corresponding to semi-major axes of 7000 km and 7400 km, spanning the likely range for most LEOs. The corresponding altitude range is approximately 640–1040 km. The figure emphasizes the secondary role of semi-major axis in determining the rate at which the orbit precesses.

We assign index 0 to the LEO and label the GPS satellites from 1 to n. The model follows the trajectories of the LEO and the GPS satellites, starting from epoch time t_0 and advancing in time steps of Δt until time t_1. The simulations span ten days in 10 s time steps. For the k^{th} satellite, the orbit model computes the following quantities:

$\mathbf{x}_k$, the position of the satellite in geocentric coordinates;

$r_k = |\mathbf{x}_k|$, the distance of the satellite from the centre of the earth;

$\mathbf{u}_k = \mathbf{x}_k / r_k$, a unit vector pointing from the centre of the earth to the satellite;

$\mathbf{t}_k$, a unit vector parallel to the velocity of the satellite;

$\mathbf{w}_k$, a unit vector parallel to $\mathbf{u}_k \times \mathbf{t}_k$;

$\mathbf{v}_k = \mathbf{w}_k \times \mathbf{u}_k$, a unit vector perpendicular to both $\mathbf{w}_k$ and $\mathbf{u}_k$, completing a right-handed system of axes centred on the satellite;

$\mathbf{q}_k$, a unit vector pointing from the LEO to the k^{th} GPS satellite,

$$\mathbf{q}_k = \frac{\mathbf{x}_k - \mathbf{x}_0}{|\mathbf{x}_k - \mathbf{x}_0|}.$$

2.2 Visibility

We let $\mathbf{m}$ denote the axis and $\theta_\star$ the horizon of the antenna, the latter defined to be the maximum angle that rays may make with $\mathbf{m}$ and still be detected by the GPS receiver. We deem a GPS satellite to be visible from the LEO if the ray connecting them is above the horizon for the antenna and does not intersect the earth. Thus, the k^{th} GPS satellite is deemed visible if

$$\theta_k \leq \theta_\star,$$

where

$$\cos\theta_k = \mathbf{m} \cdot \mathbf{q}_k.$$

Refraction in the atmosphere is neglected in this step, but the omission has negligible effect upon the conclusions of this report.

In order to decide whether GPS satellite k is occulted by the earth, we consider a ray with length α starting at $r_0\mathbf{u}_0$ (the LEO) and pointing in direction $\mathbf{q}_k$ towards the k^{th} GPS satellite. This ray will intersect the earth if the vector

$$\mathbf{h}_k = r_0\mathbf{u}_0 + \alpha\mathbf{q}_k$$

from the centre of the earth to the end point of the ray has components that satisfy the equation defining the spheroidal surface of the earth. Such is the case if α satisfies the quadratic equation

$$r_0^2 P + 2\alpha r_0 R + \alpha^2 Q = a_e^2, \tag{1}$$

where

$$P = u_1^2 + u_2^2 + u_3^2(a_e/b_e)^2,$$

$$Q = q_1^2 + q_2^2 + q_3^2(a_e/b_e)^2,$$

and

$$R = u_1 q_1 + u_2 q_2 + u_3 q_3 (a_e/b_e)^2.$$

In these expressions, a_e and b_e denote the semi-major and semi-minor axes of the earth and u_j and q_j denote the components of $\mathbf{u}_0$ and $\mathbf{q}_k$. Equation (1) has two real solutions if

$$\Delta = R^2 - Q(P - a_e^2/r_0^2) > 0, \tag{2}$$

so the ray intersects the earth when condition (2) is satisfied, and misses otherwise. The required solution for α is

$$\alpha = \frac{r_0}{Q}(|R| - \sqrt{\Delta}).$$

2.3 Quality of the GPS configuration

We use 'geometrical dilution of precision', denoted by $\mathcal{G}$, as a measure of the quality of the configuration of visible GPS satellites for determining the position and velocity of the LEO. Following Spilker, Jr. (1996), we define

$$\mathcal{G} = \text{trace}(G^\star G),$$

where G is the matrix representing the sensitivity of pseudoranges to uncertainties in GPS satellite positions and GPS clock biases. The matrix G is given by

$$G = \begin{pmatrix} \mathbf{q}_{k_1} & 1 \\ \mathbf{q}_{k_2} & 1 \\ \cdots & \cdot \\ \mathbf{q}_{k_{N_v}} & 1 \end{pmatrix}$$

where $k_1, k_2, \ldots, k_{N_v}$ label the GPS satellites visible from the LEO, N_v in number. The unit vectors $\mathbf{q}_{k_1}, \mathbf{q}_{k_2}, \ldots, \mathbf{q}_{k_{N_v}}$ are regarded as row vectors, so G is an $(N_v \times 4)$ matrix. It is straightforward to deduce that

$$\mathcal{G} = \sum_{l=1}^{4} s_l^{-2},$$

where s_1, s_2, s_3 and s_4 are the singular values of G. We expect that accuracy of navigation will be high when $\mathcal{G}$ is small, and vice-versa.

2.4 Setting satellites and GPS underflights

We deem a GPS satellite to be setting if it is visible at one time step but occulted by the earth at the next. Setting satellites are only counted if they are contained within a cone centred on the (negative) velocity axis of the LEO with vertex angle $\zeta_\star$. Thus, we count GPS satellite k as setting if

$$\zeta_k \leq \zeta_\star \quad \text{or} \quad \zeta_k \geq \pi - \zeta_\star,$$

where

$$\cos\zeta_k = -\mathbf{t}_0 \cdot \mathbf{q}_k.$$

		Configuration			
		1	2	3	4
Number of antennas		1	1	2	1
Antenna direction	$\mathbf{m}$	Rearward	Rotating	Inclined	Upward
Frequency of rotation	ν	0	144	144	Irrelevant
Visibility cone angle	$\theta_\star$	90°	90°	90°	120°
Setting cone angle	$\zeta_\star$	45°	45°	45°	45°
Overhead cone angle	$\chi_\star$	10°	10°	10°	10°

Table 3: Antenna configurations. Frequency of rotation is expressed in revolutions per day.

Similarly, we deem GPS satellites to be overhead if they lie within a cone centred on the position axis with vertex angle $\chi_\star$. Thus, we count GPS satellite k as overhead if

$$\chi_k \leq \chi_\star,$$

where

$$\cos \chi_k = \mathbf{u}_0 \cdot \mathbf{q}_k.$$

2.5 Antenna configurations

In order to promote better thermal regulation of the payload, it is probable that the LEO will rotate slowly about its $\mathbf{u}_0$ axis with frequency ν. As an indication of the frequency, we note that a micro-satellite commissioned by the US Air Force from the University of Surrey completes a full revolution every 10 minutes.

We consider the four antenna configurations outlined in the introduction and summarized in table 3. The antenna axes are expressed in terms of the local coordinate axes for the LEO as follows:

$$\mathbf{m} = \begin{cases} -\mathbf{v}_0 & \text{in case 1} \\ -\mathbf{p} & \text{in case 2} \\ (\mathbf{u}_0 \pm \mathbf{p})/\sqrt{2} & \text{in case 3} \\ \mathbf{u}_0 & \text{in case 4} \end{cases},$$

where $\mathbf{p}$ denotes a unit vector in the horizontal plane rotating with the bus,

$$\mathbf{p} = -\cos 2\pi\nu(t - t_0)\, \mathbf{v}_0 + \sin 2\pi\nu(t - t_0)\, \mathbf{w}_0.$$

In configuration 2, the antenna axis points back along the satellite track at epoch, but thereafter rotates about the $\mathbf{u}_0$ axis with frequency ν. In configuration 3, the twin antennas are inclined at 45° to the vertical, but are 180° apart in azimuth. Both antennas rotate with the bus. The value $\theta_\star = 120°$ for configuration 4 represents the practical minimum if an upward pointing antenna on the LEO is to observe any occultations. This is easily confirmed by finding the angle at which a ray from the LEO is tangential to the earth.

3 Results

We begin by considering the impact of orbit inclination upon the spatial distribution of occultations and showing that the requirement that occultations should be distributed uniformly over the globe limits the inclination to two narrow ranges. Although we will show results for only one antenna configuration over the range $0° \leq i \leq 180°$, the conclusion is valid for all. This finding allows us to focus on the restricted range of inclinations for the remainder of the report.

Figures 3 and 4 show the spatial distribution of occultations for configuration 1 with rearward pointing antenna, semi-major axis 7200 km, and right ascension of the ascending node $\Omega = 30°$ at epoch. The panels on the left show the spatial distributions for inclinations increasing from 0° to 90°, while the panels on the right correspond to inclinations decreasing from 180° to 90°. The horizontal axis in each panel is the longitude λ of the occultation, while the vertical axis is not latitude ϕ but $\sin\phi$, varying from -1 to $+1$. Because space on the vertical axis is limited, only labels corresponding to $\pm 60°$, $\pm 30°$ and 0° are marked. The choice of $\sin\phi$ for the vertical coordinate ensures that a uniform distribution of occultations, with equal numbers in equal areas of the globe, would appear as a uniform distribution of points in the plots.

We see in figures 3 and 4 that the distribution of occultations is localized near the equator for both low and high inclination orbits, but diffuses towards the poles as the inclination approaches 90°. For inclinations in the ranges $0° \leq i < 50°$ and $130° < i \leq 180°$, the polar regions are unsampled, while occultations over the equatorial and mid-latitude regions are noticeably sparse for inclinations in the range $70° < i < 110°$. The situation is similar for all antenna configurations. Therefore, we will focus henceforth on the range $50° \leq i \leq 70°$ and its supplementary range $110° \leq i \leq 130°$.

3.1 Number of visible satellites, N_v

Figure 5 presents histograms of the number of GPS satellites visible from the LEO for the configuration with rearward pointing antenna. The histograms are based on calculations at 10 s time steps over a ten-day period. The figure has ten panels, labelled by the inclination i of the orbit, and each panel has five histograms, corresponding to five values of Ω, the right ascension of the ascending node at epoch. The semi-major axis of the LEO orbit is 7200 km. The figure shows that the number of visible GPS satellites changes little with either inclination or right ascension of the ascending node of the LEO orbit. As the inclination approaches 90°, the distribution with $\Omega = 60°$ becomes more peaked and the modal value increases slightly, although the increase is unlikely to be significant. The probability that the number of visible satellites will be five or less is not negligible, and the consequence is evident in figure 6 where the distribution of $\mathcal{G}$ is seen to have a long tail of high values, indicating lower potential for accurate orbit determination. The modal value of $\mathcal{G}$ is approximately 1.6.

Because the distributions of N_v and $\mathcal{G}$ vary little with the inclination of the orbit, we show in figure 7 only the distributions for $i = 60°$ for the other antenna configurations.

Histograms for the number of visible GPS satellites for configuration 2 with rotating antenna appear to be gaussian. The modal value of N_v is approximately 7.5, but the

fraction of time with fewer than five GPS satellites visible is significant. Distributions of $\mathcal{G}$ are marginally broader than those for antenna configuration 1, with greater probability of unfavourable GPS configurations.

Configuration 3 has twin antennas inclined at 45° to the vertical and separated in azimuth by 180°. Consequently, we expect this configuration to observe more GPS satellites, and this is apparent in figure 7 which shows that the modal value of N_v is approximately 15. The distribution of $\mathcal{G}$ in figure 7 is much narrower, with modal value approximately equal to 0.8, so this configuration is likely to be very favourable for determining the LEO orbit.

Configuration 4 with an upward pointing antenna observes the largest number of GPS satellites, as shown by the histograms in figure 7. The number of visible GPS satellites varies between 10 and 20, with the modal value approximately equal to 17. The distribution of $\mathcal{G}$ is narrow and the modal value is low (≈ 0.8), so we expect excellent determination of the orbit of the LEO with this configuration.

3.2 Number of setting satellites, N_s

Figure 8 shows the number N_s of setting occultations per day for the four antenna configurations. In each panel of the figure, N_s is plotted as a function of the inclination i of the orbit for five values of Ω, the right ascension of the ascending node. Only occultations within 45° of the satellite track have been counted, for the reason already outlined. The figures show that the number of setting satellites changes little with inclination or right ascension of the ascending node at epoch. Because the setting satellites occur in the rearward hemisphere, configurations 1 and 4 with rearward and upward pointing antennas observe the same occultations. Configuration 2 with antenna rotating in the horizontal plane sees approximately half as many occultations, simply because the hemispherical field of view of the rotating antenna overlaps the cone from which occultations are accepted for only half the time. Configuration 3 with twin antennas is only marginally better because, while one antenna is pointing into the rearward hemisphere, the other is pointing forward into the hemisphere where no occultations occur. Consequently, the primary advantage of the twin antenna configuration is improved navigation of the LEO, and not a doubling of the number of setting occultations.

3.3 Spatial distributions of occultations

We now turn to the dependence of the spatial distribution of occultations upon the antenna configuration, inclination the LEO orbit and right ascension of the ascending node at epoch. However, to avoid repetition of similar diagrams, we will show plots for only two orbit inclinations ($i = 60°$ and $i = 120°$), even though in the text we refer to other inclinations. We have noted already that there is a general pattern of poleward diffusion of the occultations with decreasing $|90 - i|$.

Figure 9 shows the spatial distribution of occultations for configuration 1 with rearward pointing antenna and orbit semi-major axis 7200 km. The panels on the left of figure 9 correspond to an orbit inclinations of 60°, while those of the right correspond to 120°. The plots within each column correspond to ascending nodes with right ascensions of 0°, 15°,

30°, 45° and 60°. Although the differences are small, the distribution with $i = 120°$ and $\Omega = 30°$ at epoch appears to be the most uniform. Note that this orbit starts at epoch in one of the six planes containing the GPS satellites, but thereafter precesses eastwards at approximately 3° per day, so that after 10 days it lies midway between two GPS planes.

Results for the antenna configurations 2 and 3 are presented in figures 10–11. The number of occultations is approximately one-half that for antenna configuration 1, but otherwise the patterns are similar. Occultations observed with configuration 4 are identical to those for configuration 1, and therefore are not shown. Generally, the orbit that is most nearly uniform has inclination $i = 120°$ and ascending node with right ascension $\Omega = 30°$ at epoch.

3.4 Time distributions of occultations

Figure 12 show the probability distributions of times of occultation for antenna configurations 1–4. Only one inclination is shown ($i = 60°$) because distributions for other inclinations are very similar. The insensitivity to inclination is simply a reflection of the regularity of the placement of the GPS navigation satellites. The distributions show that the times of occultation are spread uniformly over the hours of the day. The small ripple superimposed on the mean value is unlikely to have any significant consequences.

3.5 Number of GPS underflights, N_o

Whenever the LEO underflies a GPS satellite, it is possible in principle to determine the free electron content of the ionosphere along the radial line between LEO and GPS satellite. In this subsection, we present distributions showing how frequently such configurations occur.

Figure 13 shows the number N_o of times per day that a GPS satellite lies within a 10° cone (half-angle) above the LEO, plotted as a function of the inclination i of the LEO orbit for five values of Ω, the right ascension of the ascending node. The number of GPS underflights has maxima when the inclination of the LEO orbit is 55° or 125°, in which cases the plane of the orbit coincides with one of the six planes containing the GPS constellation.

The spatial distribution of underflights is shown in figures 14 and 15 for inclinations of the LEO orbit ranging from 0° to 180° and right ascension of the ascending node $\Omega = 30°$ at epoch. For 0° and 180° inclination, the underflights are confined to the equator. For polar orbits with inclination 90°, there are no underflights within a latitude band from approximately 20° S to 20° N. The orbit that gives the most uniform distribution of occultations has a sparse distribution of underflights confined to the latitude band from 60° S to 60° N. Spatial distributions of underflights for orbits with $\Omega = 0, \ldots, 60°$ at epoch are similar in form.

4 Conclusions

We have tracked a low earth orbiting satellite (LEO) and the GPS constellation to determine:

1. the number of GPS satellites visible from the LEO;
2. the suitability of the visible GPS constellation for precise determination of the LEO orbit;
3. the number and spatial distribution of occultations of GPS satellites by the earth;
4. the number and spatial distribution of underflights of GPS satellites by the LEO.

Four GPS antenna configurations and 105 orbits were considered for the LEO.

Configuration 4 with upward pointing GPS antenna offers the highest number of visible GPS satellites for navigation, the lowest geometrical dilution of precision $\mathcal{G}$, and the highest number of occultations per day. These results are independent of rotation of the satellite about its vertical axis. However, the configuration assumes that the GPS antenna has very wide field of view and can detect rays from directions at 120° to the antenna axis. Whether such an antenna is technically feasible is an open question.

Of the configurations with the antenna axis in the horizontal plane, the case without rotation observes approximately twice as many occultations per day as the rotating case, and therefore is preferable. If other considerations (such as thermal control) dictate that the LEO must rotate, then the performance for GPS meteorology could be improved with two orthogonal antennas, rather than just the one assumed in this report.

An orbit with inclination $i \approx 60°$ or 120° offers the most uniform distribution of occultations over the globe. Inclinations below 50° or above 70° give unacceptable coverage of the polar and equatorial regions, respectively. For an orbit with $i = 60°$ or $i = 120°$, the rate of precession of the orbit plane is approximately 3° per day, and so the constellation of GPS satellites and LEO will repeat after approximately 20 days. The precise repeat time would be determined by specifying the semi-major axis of the orbit.

The number of underflights of GPS satellites by the LEO is maximized if the inclination of the LEO orbit is either 55° or 125°. The distribution of underflights is contained in a latitude band bounded by the inclination of the orbit. For near polar orbits, there are long periods (exceeding ten days) when the LEO never underflies a GPS satellite in a wide latitude band centred on the equator.

References

Brouwer, D., and G. M. Clemence, 1961: *Celestial mechanics.* Academic Press, New York.

Eyre, J. R., 1994: Assimilation of radio occultation measurements into a numerical weather prediction system. Technical memorandum 199, European Centre for Medium-Range Weather Forecasts.

Gorbunov, M. E., 1996: Three-dimensional satellite refractive tomography of the atmosphere: numerical simulation. *Radio Science*, **31**, 95–104.

Hajj, G. A., E. R. Kursinski, W. I. Bertinger, S. S. Leroy, T. K. Meehan, L. J. Romans, and J. T. Schofield, 1995: Initial results of GPS-LEO occultation measurements of earth's atmosphere obtained with the GPS-MET experiment. *IAG Symposium G1: GPS trends in precise terrestrial, airborne, and spaceborne applications*, Boulder Co. IUGG XXI General Assembly.

Kursinski, E. R., G. A. Hajj, W. I. Bertinger, S. S. Leroy, T. K. Meehan, L. J. Romans, J. T. Schofield, D. J. McCleese, W. G. Melbourne, C. L. Thornton, T. P. Yunck, J. R. Eyre, and R. N. Nagatani, 1996: Initial results of radio occultation observations of earth's atmosphere using GPS. *Science*, **271**, 1107–1110.

Spilker, Jr., J. J., 1996: Global positioning system: Theory and applications. *Progress in astronautics and aeronautics, volume 1*, B. W. Parkinson and J. J. Spilker, Jr., Eds. 163.

Melbourne, W. G., E. S. Davis, C. B. Duncan, G. A. Hajj, K. R. Hardy, E. R. Kursinski, T. K. Meehan, L. E. Young, and T. P. Yunck, 1994: The application of spaceborne GPS to atmospheric limb sounding and global change monitoring. JPL Publication 94-18, NASA, Jet Propulsion Laboratory, Pasadena, California.

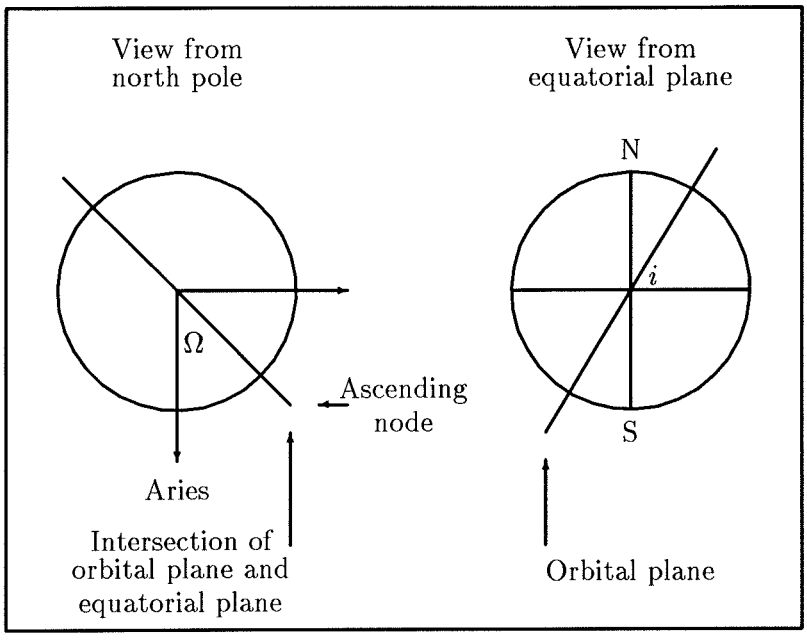

Figure 1: The left hand figure shows the intersection of the orbital plane and the equatorial plane as seen from the north pole. Aries is the direction defined by the intersection of the earth's equatorial plane and the plane of the earth's orbit around the sun. The angle marked Ω is the right ascension of the ascending node. The right hand figure shows the view from within the equatorial plane. The angle marked i at which the orbital plane of the satellite cuts the equatorial plane is the inclination of the orbit.

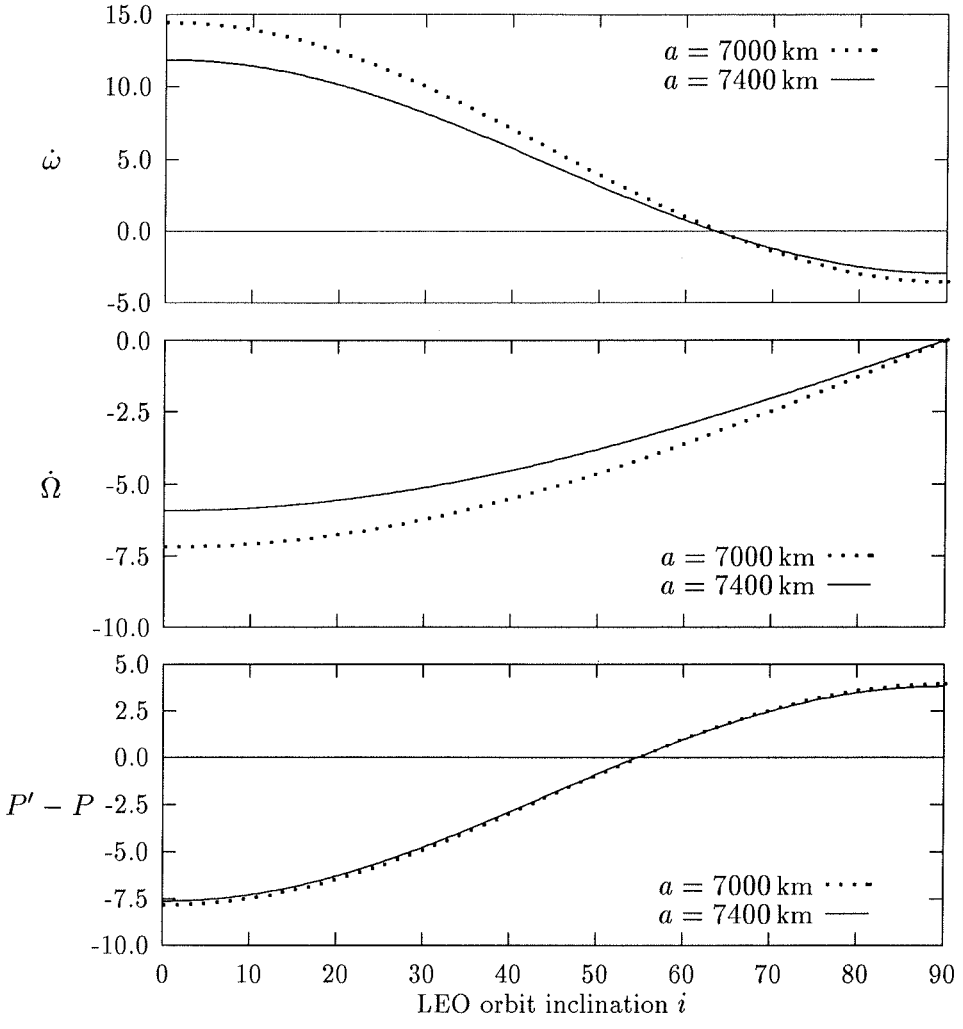

Figure 2: The upper panel shows $\dot{\omega}$, the rate of precession of the argument of perigee in degrees per day, for two values of the semi-major axis a as a function of i, the inclination of the LEO orbit. The middle panel shows $\dot{\Omega}$, the rate of precession of the right ascension of the ascending node in degrees per day. The bottom panel shows $P' - P$, the difference in seconds between the anomalistic period and the period for elliptical motion in a central potential.

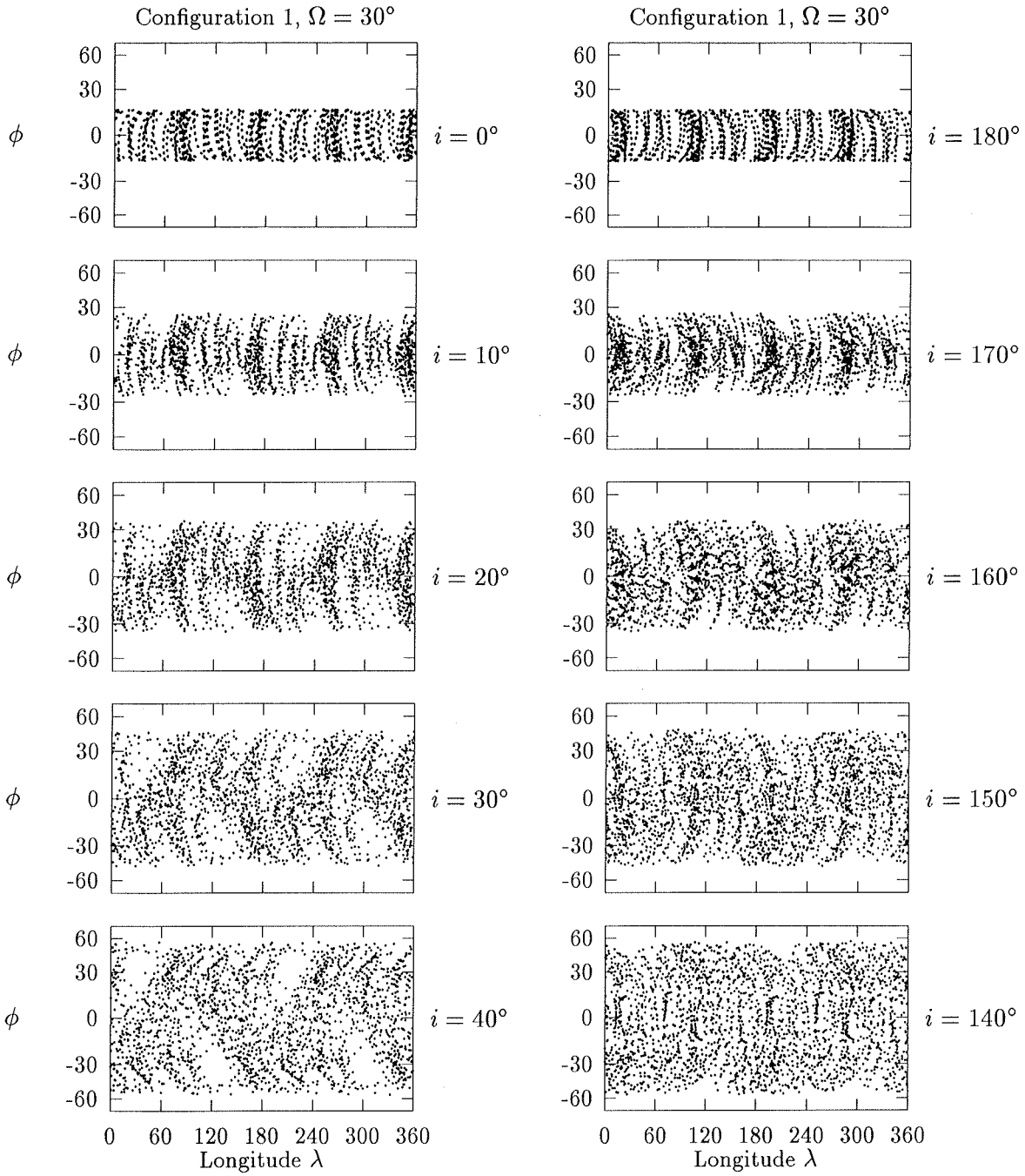

Figure 3: Spatial distribution of GPS occultations in a ten-day period for configuration 1 with rearward pointing GPS antenna. In this model, the LEO is assumed to be non-rotating. Only occultations within 45° of the satellite track have been included. The panels on the left correspond to inclinations of 0°–40°, while those on the right correspond to 180°–140°. The right ascension of the ascending node at epoch is 30°.

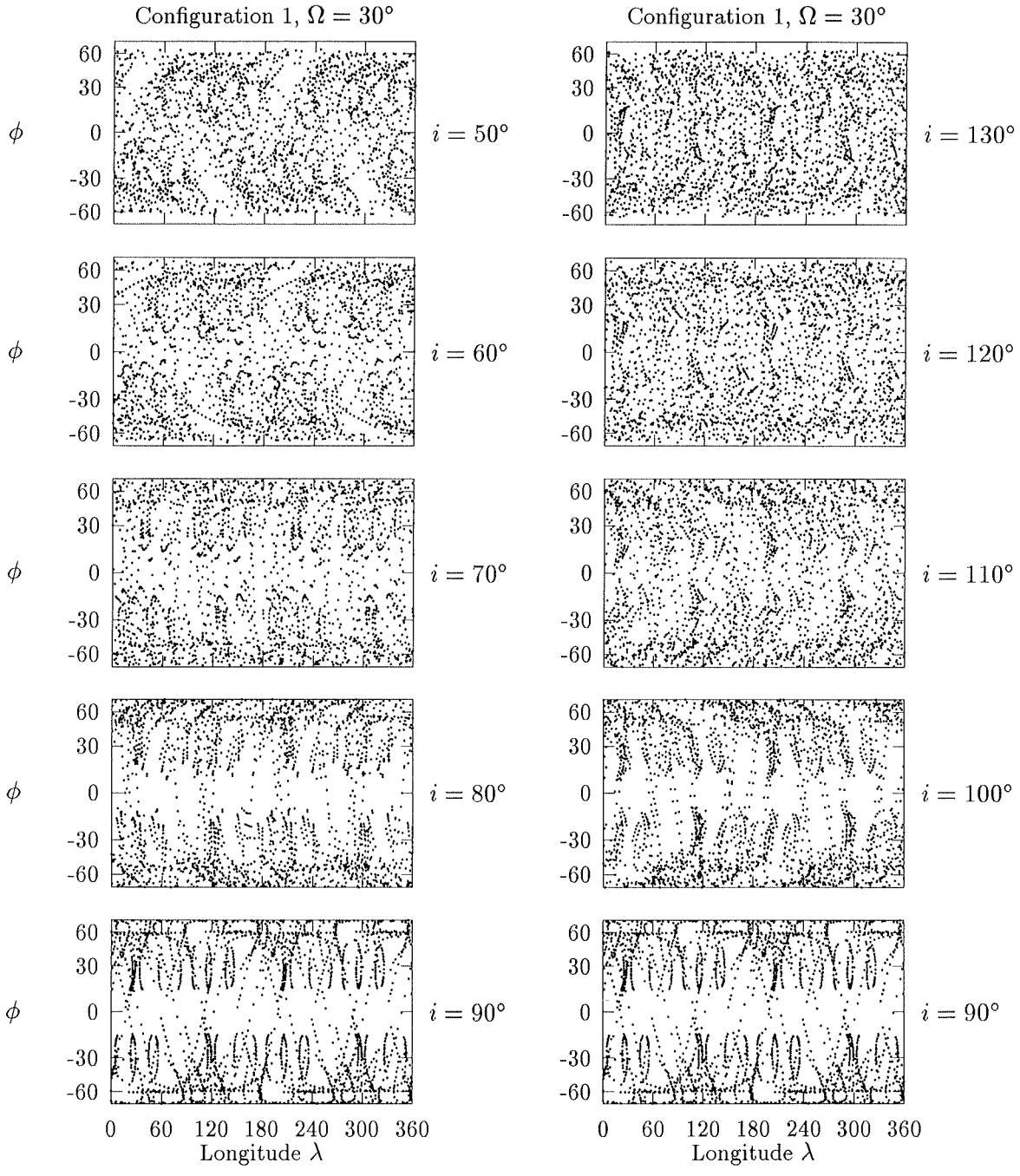

Figure 4: Spatial distribution of GPS occultations in a ten-day period for configuration 1 with rearward pointing GPS antenna. In this model, the LEO is assumed to be non-rotating. Only occultations within 45° of the satellite track have been included. The panels on the left correspond to inclinations of 50°–90°, while those on the right correspond to 130°–90°. The right ascension of the ascending node at epoch is 30°.

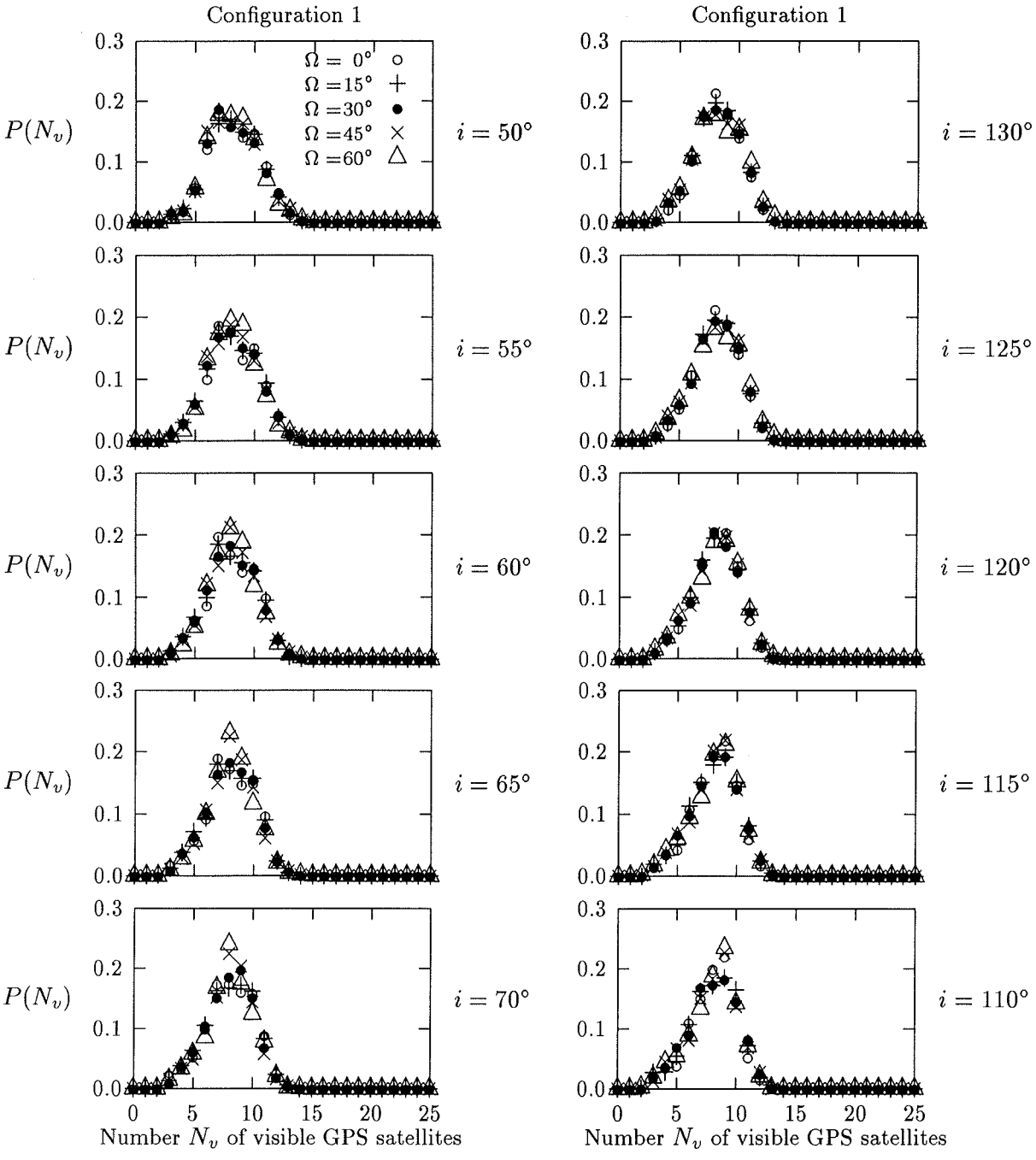

Figure 5: Probability distribution $P(N_v)$ for the number N_v of GPS satellites visible from the LEO with rearward pointing antenna. The areas under the histograms are normalized to unity. The panels on the left correspond to inclinations of 50°–70°, while those on the right correspond to 130°–110°. The right ascension of the ascending node at epoch takes the values indicated in the top left panel.

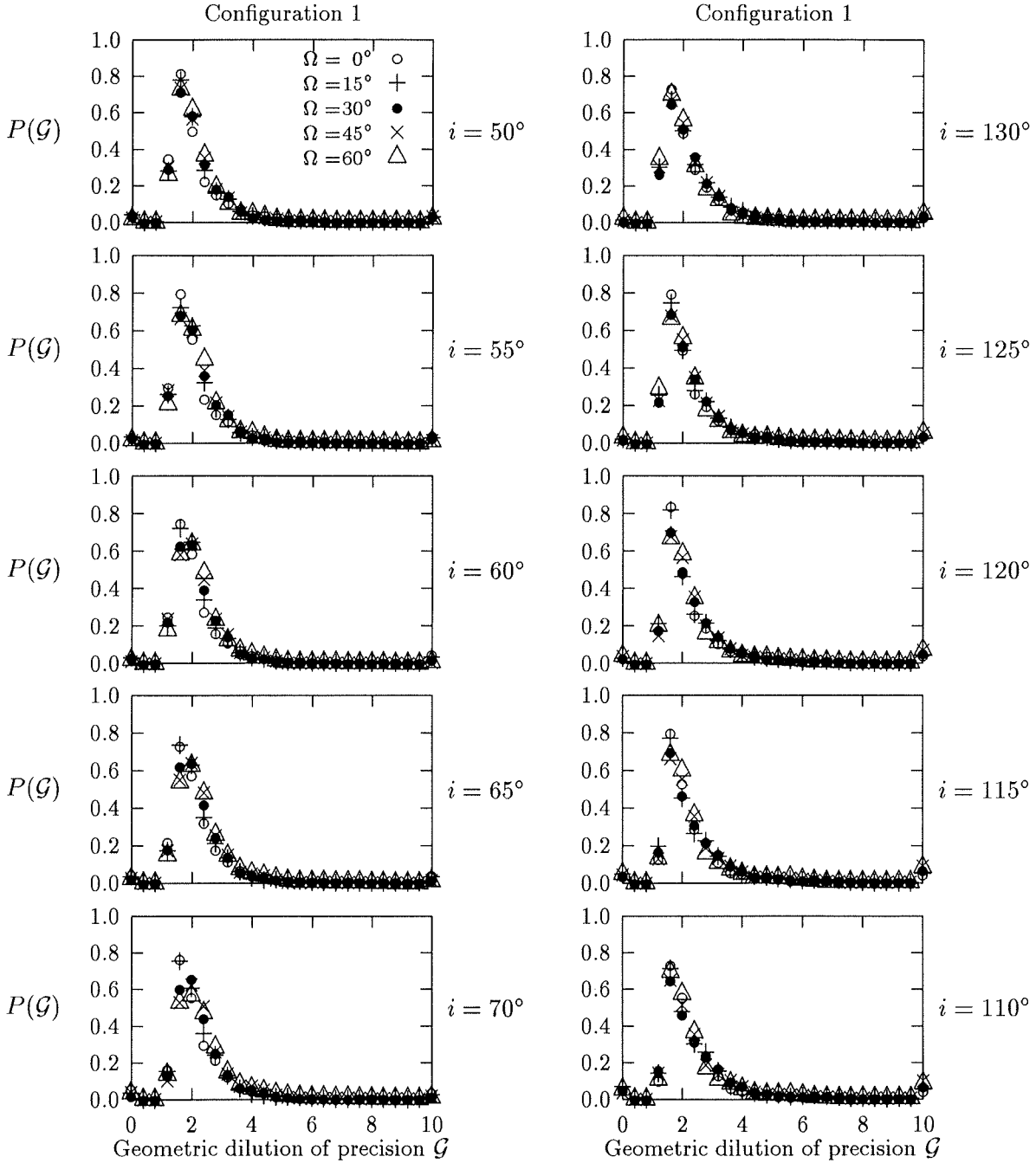

Figure 6: Probability distribution $P(\mathcal{G})$ for the geometric dilution of precision $\mathcal{G}$ of the configuration of GPS satellites visible from the LEO with rearward pointing antenna. The areas under the histograms are normalized to unity. The panels on the left correspond to inclinations of 50°–70°, while those on the right correspond to 130°–110°. The right ascension of the ascending node at epoch takes the values indicated in the top left panel.

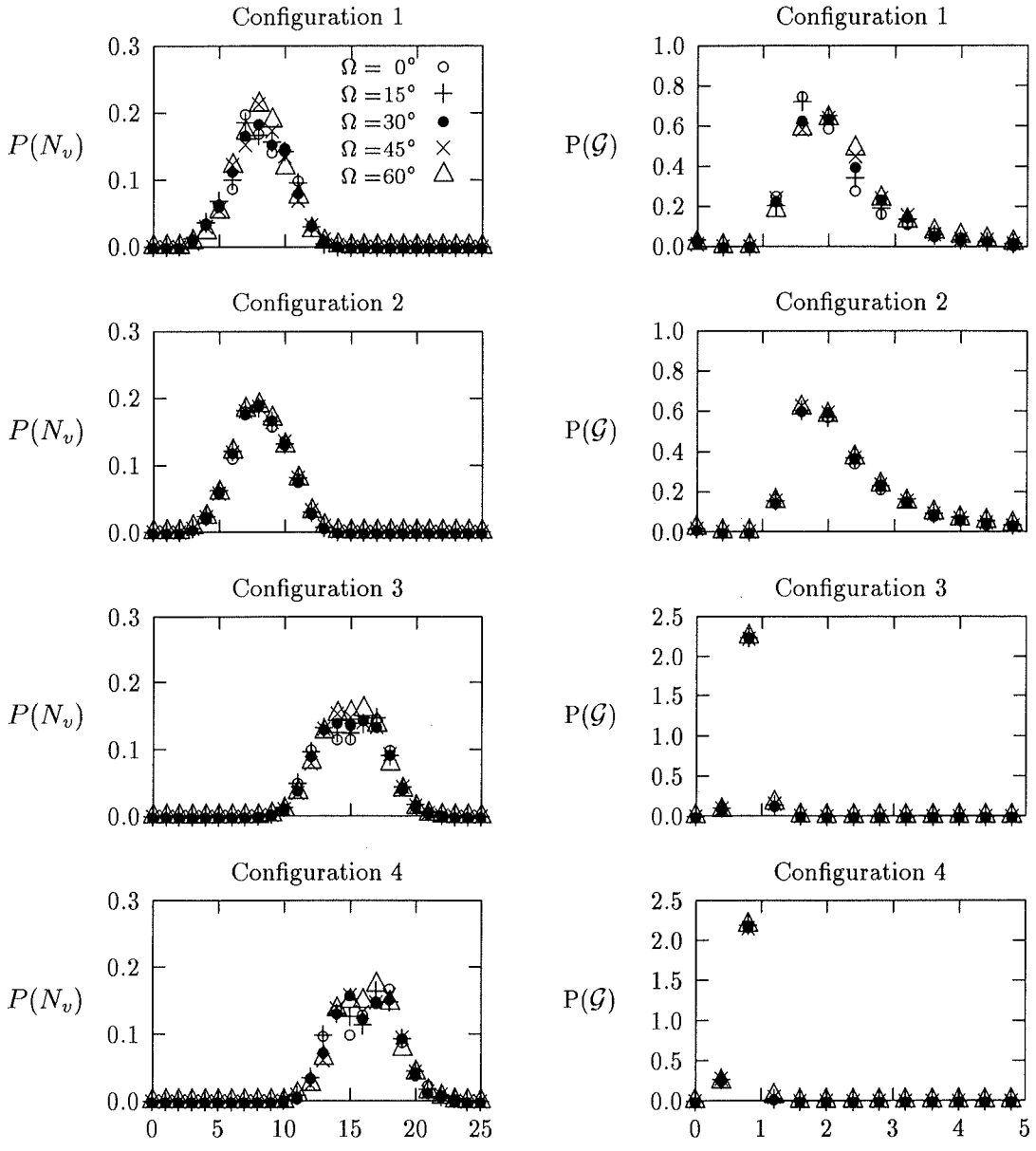

Figure 7: Probability distributions of the number of visible satellites (N_v) and the geometrical dilution of precision ($\mathcal{G}$) for all four antenna configurations. The inclination of the orbit is fixed at $i = 60°$, while the right ascension of the ascending node at epoch takes the values indicated in the top left panel.

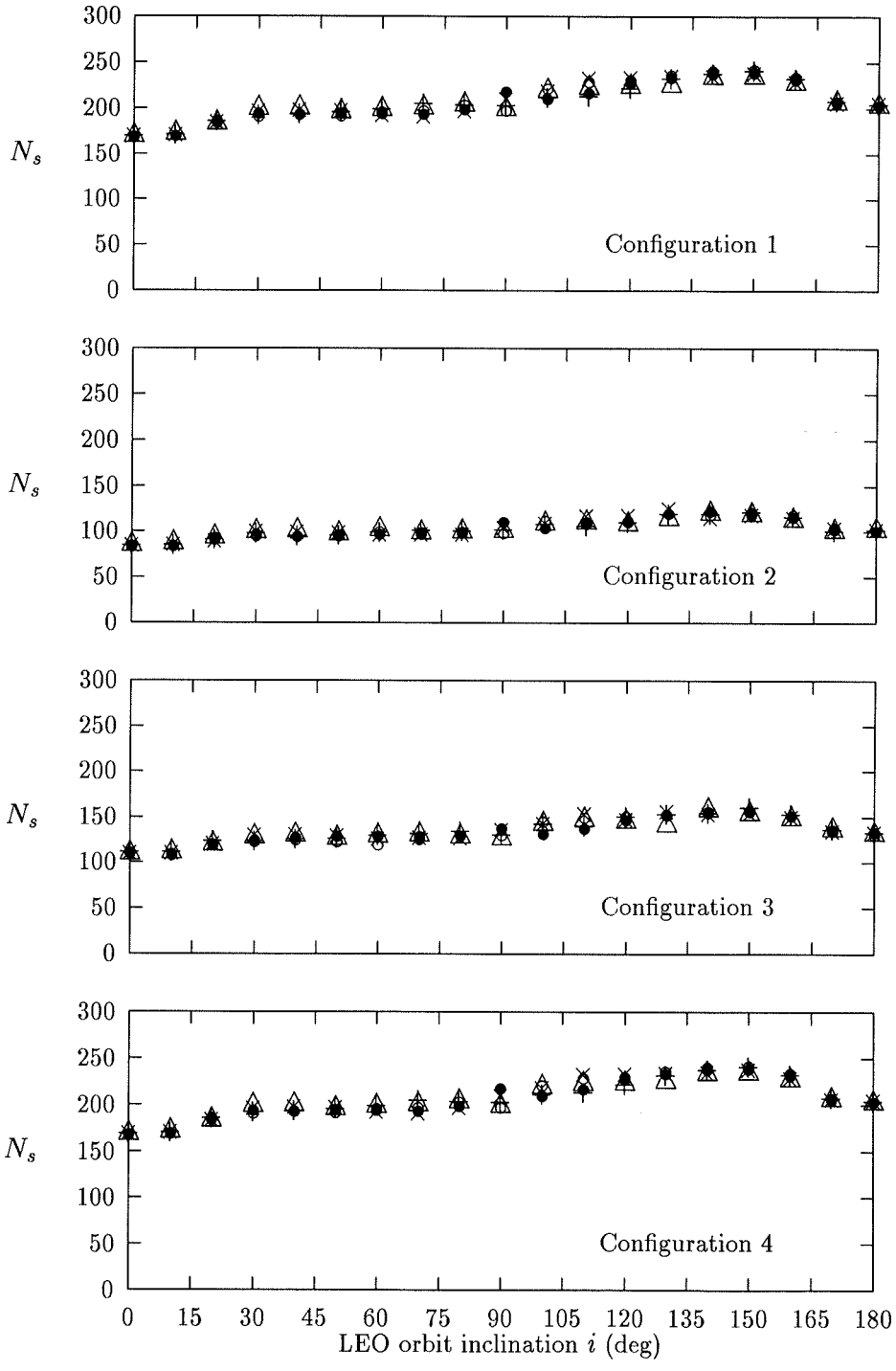

Figure 8: Number N_s of setting satellites observed per day as a function of the inclination of the LEO orbit for the four antenna configurations. The right ascension of the ascending node at epoch takes the values 0°–60°, with the same symbols as used previously.

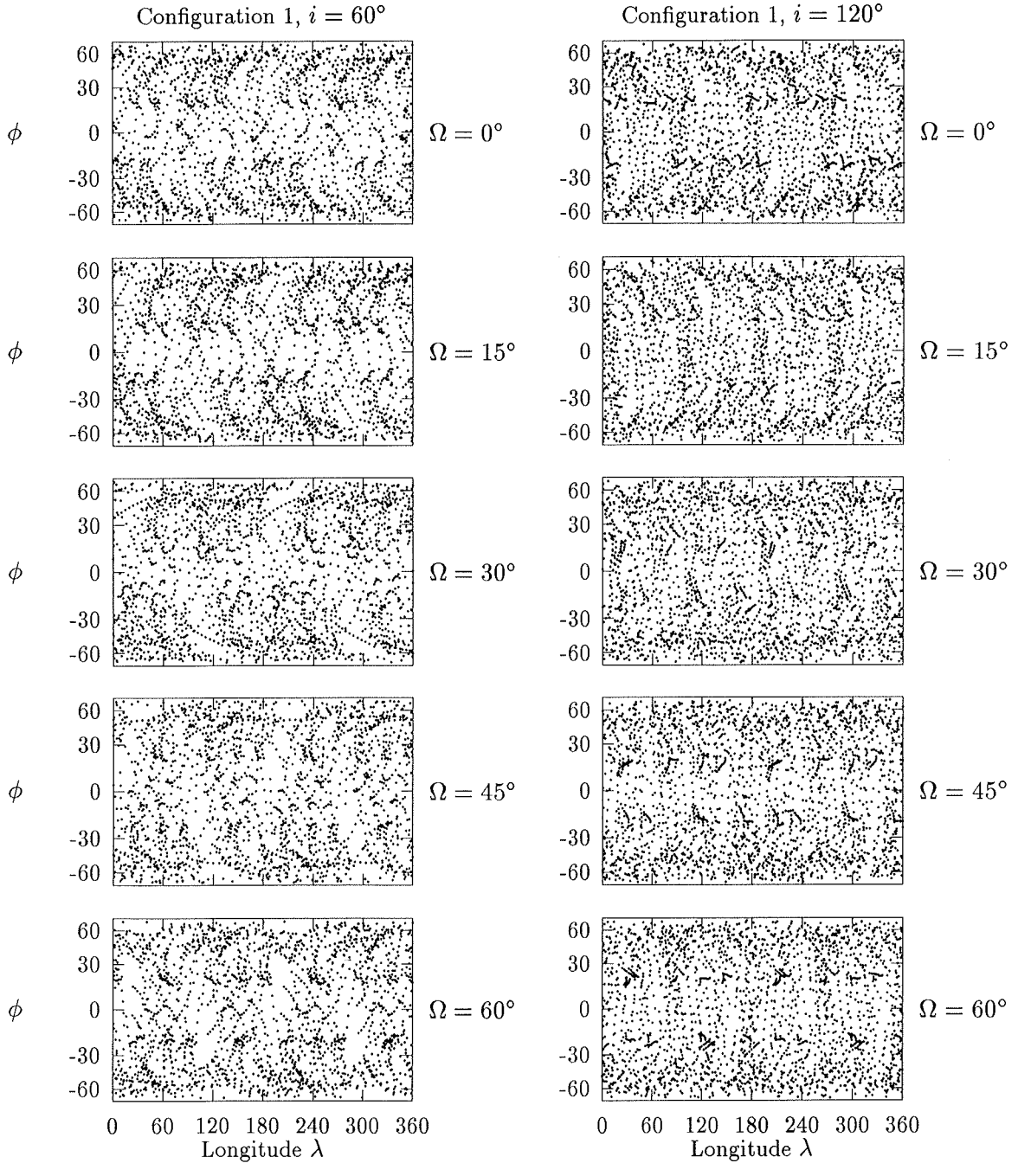

Figure 9: Spatial distribution of GPS occultations in a ten-day period for configuration 1 with rearward pointing GPS antenna. In this model, the LEO is assumed to be non-rotating. Only occultations within 45° of the satellite track have been included. The panels on the left have inclination $i = 60°$, while those on the right have $i = 120°$. In each column, the right ascension of the ascending node at epoch takes values of 0°–60°.

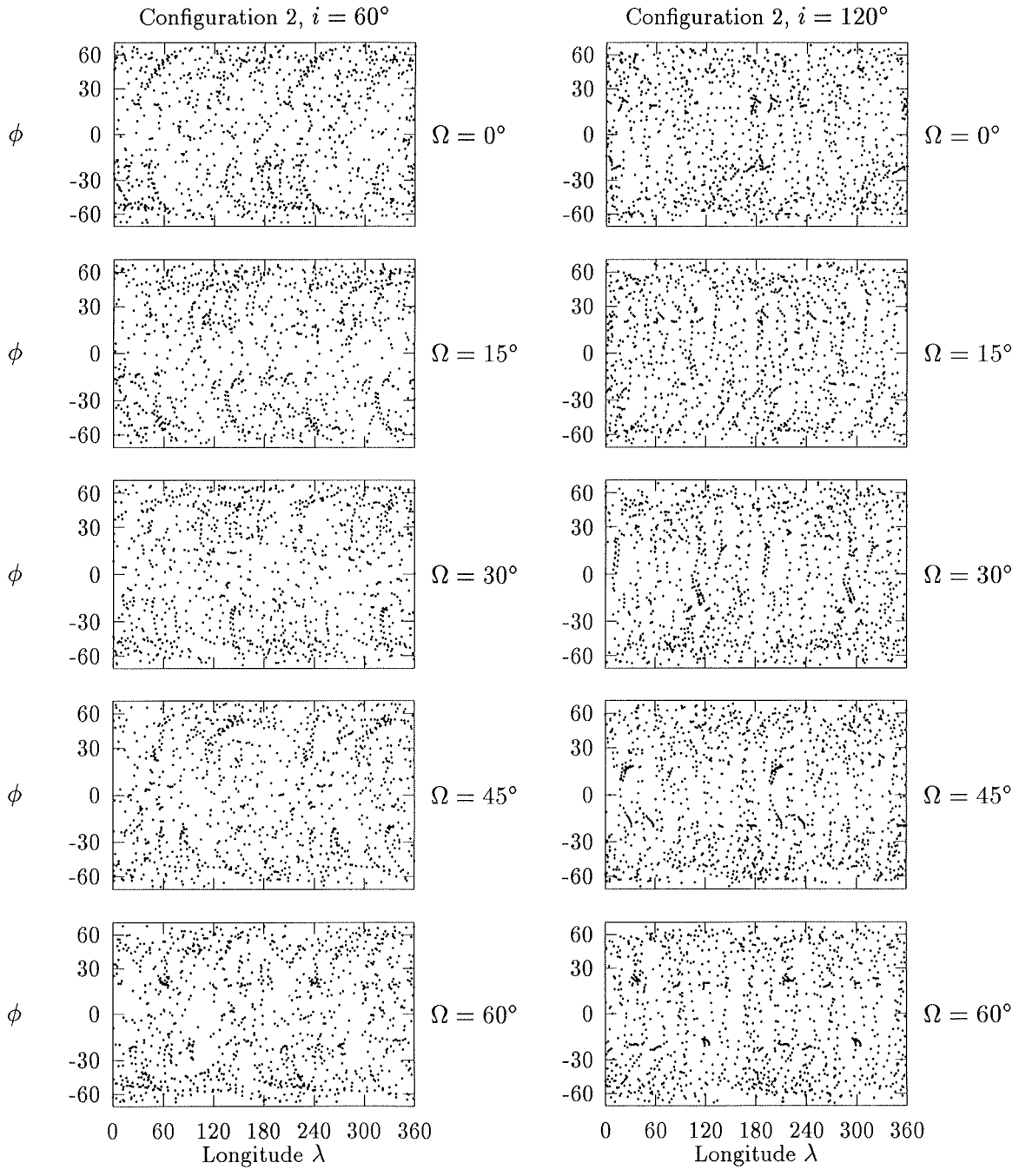

Figure 10: Spatial distribution of GPS occultations in a ten-day period for configuration 2 with horizontal antenna that rotates with the LEO once every 10 minutes. Only occultations within 45° of the satellite track have been included. The panels on the left have inclination $i = 60°$, while those on the right have $i = 120°$. In each column, the right ascension of the ascending node at epoch takes values of 0°–60°.

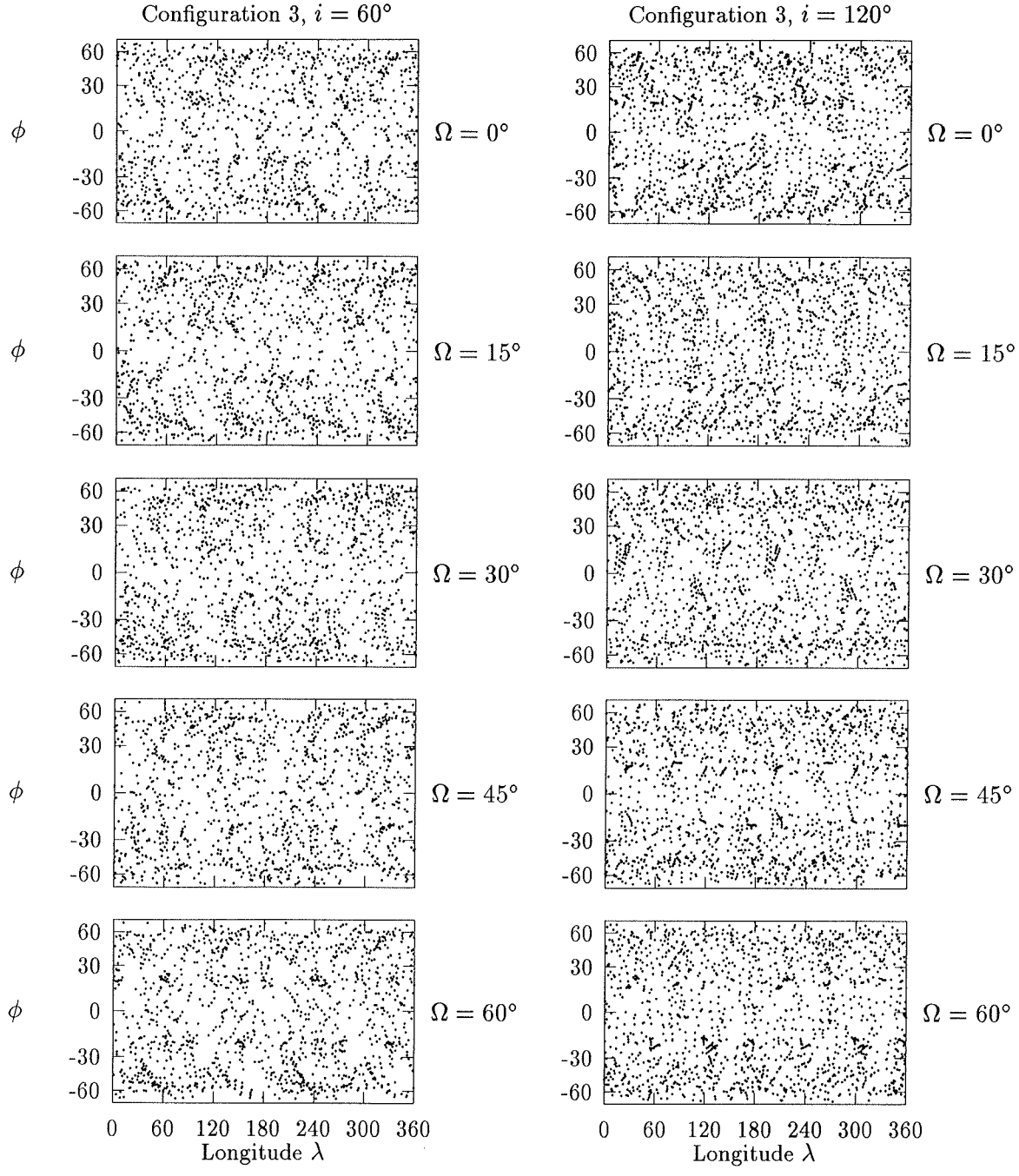

Figure 11: Spatial distribution of GPS occultations in a ten-day period for configuration 3 with two GPS antennas inclined at 45° to the position vector of the LEO, but separated in azimuth by 180°. The LEO is assumed to rotate about its position vector once every 10 minutes. Only occultations within 45° of the satellite track have been included. The panels on the left have inclination $i = 60°$, while those on the right have $i = 120°$. In each column, the right ascension of the ascending node at epoch takes values of 0°–60°.

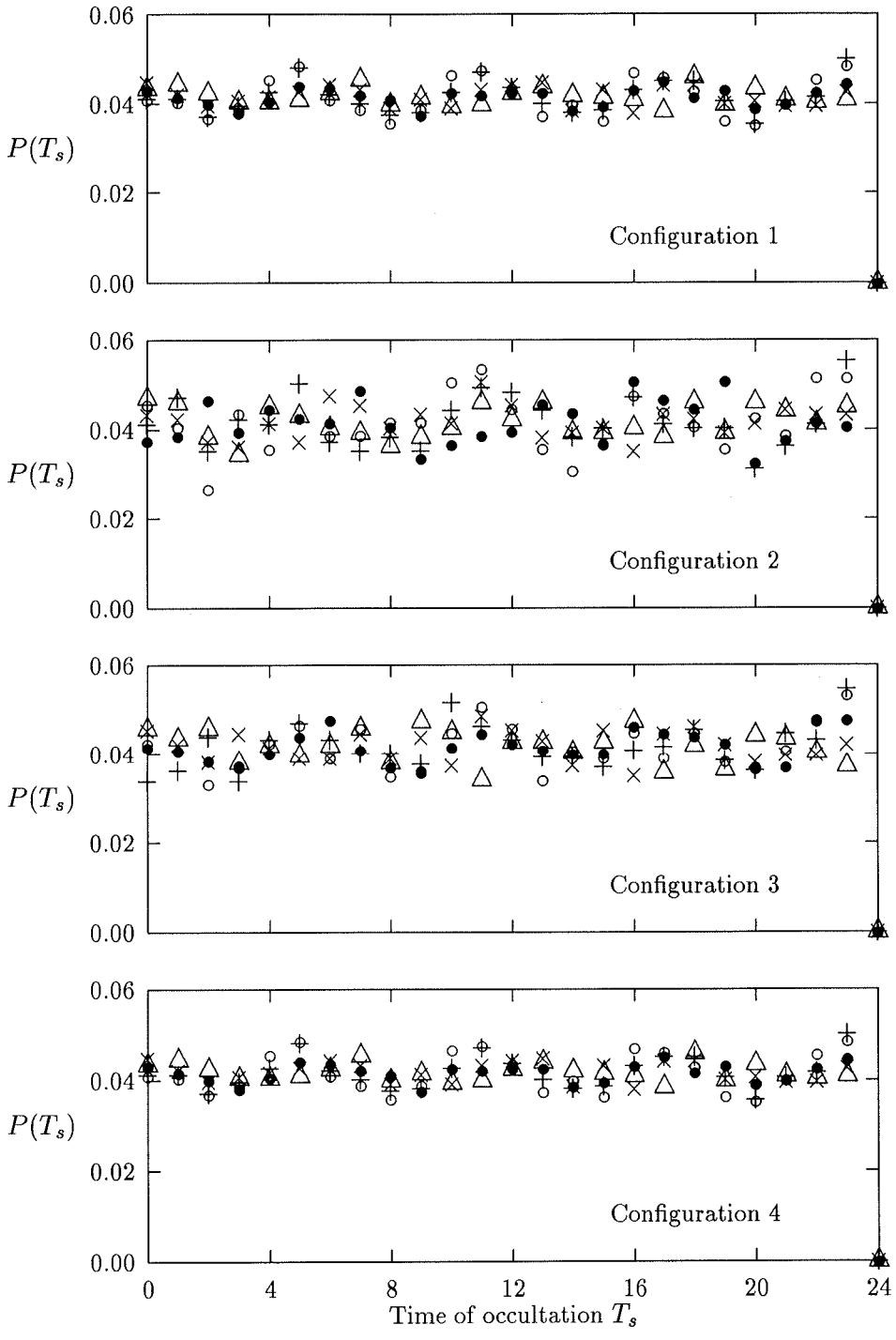

Figure 12: Probability distributions $P(T_s)$ for the time T_s of occultations visible from the LEO for all four antenna configurations. The areas under the histograms are normalized to unity. The orbit inclination is $i = 60°$, while the right ascension of the ascending node at epoch takes the values 0°–60°, with the same symbols as used previously.

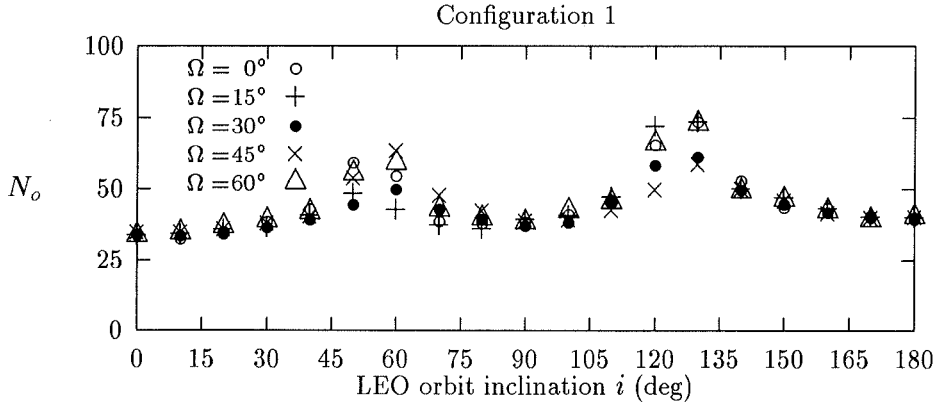

Figure 13: Number N_o of GPS underflights per day as a function of the inclination of the LEO orbit.

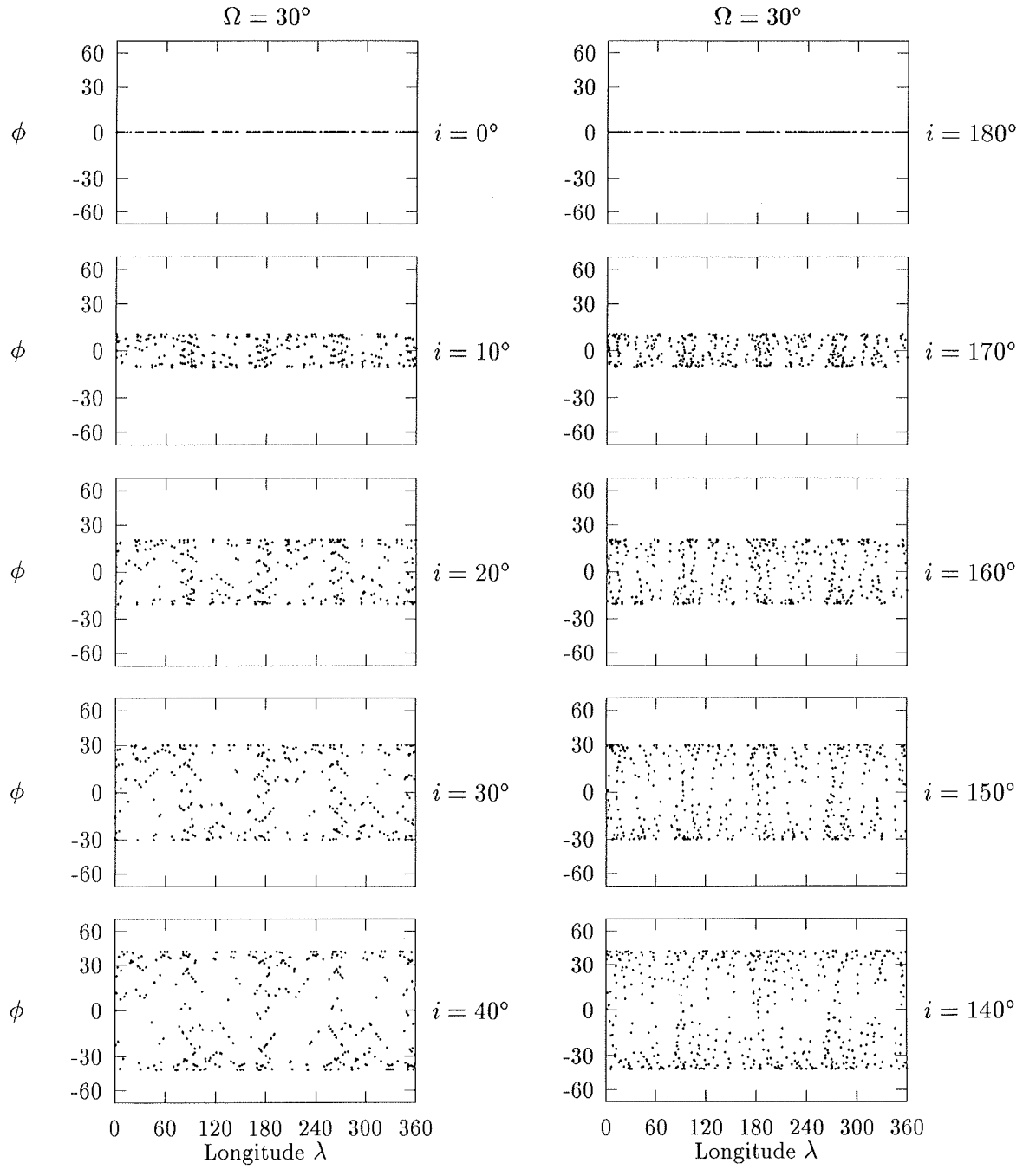

Figure 14: Spatial distribution of GPS underflights in a ten-day period. The panels on the left correspond to inclinations of 0°–40°, while those on the right correspond to 180°–140°. The right ascension of the ascending node at epoch is 30°.

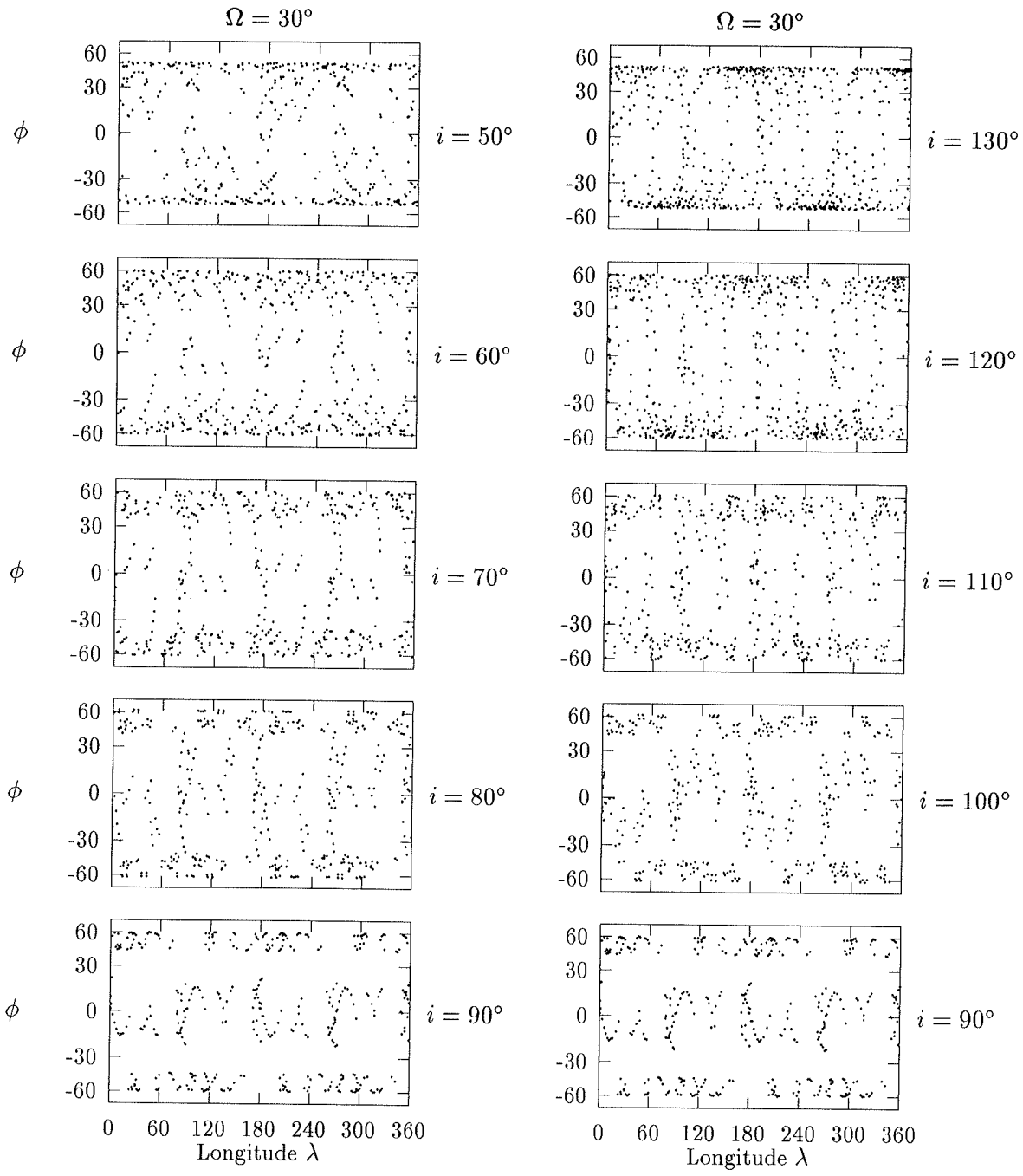

Figure 15: Spatial distribution of GPS underflights in a ten-day period. The panels on the left correspond to inclinations of 50°–90°, while those on the right correspond to 130°–90°. The right ascension of the ascending node at epoch is 30°.

CSIRO ATMOSPHERIC RESEARCH TECHNICAL PAPERS

(Series title changed from CSIRO Division of Atmospheric Research Technical Papers at number 38)

No. 1 Galbally, I. E.; Roy, C. R.; O'Brien, R. S.; Ridley, B. A.; Hastie, D. R.; Evans, W. J. F.; McElroy, C. T.; Kerr, J. B.; Hyson, P.; Knight, W.; Laby, J. E. *Measurements of trace composition of the Austral stratosphere: chemical and meteorological data.* 1983. 31 p.

No. 2 Enting, I. G. *Error analysis for parameter estimates from constrained inversion.* 1983. 18 p.

No. 3 Enting, I. G.; Pearman, G. I. *Refinements to a one-dimensional carbon cycle model.* 1983. 35 p.

No. 4 Francey, R. J.; Barbetti, M.; Bird, T.; Beardsmore, D.; Coupland, W.; Dolezal, J. E.; Farquhar, G. D.; Flynn, R. G.; Fraser, P. J.; Gifford, R. M.; Goodman, H. S.; Kunda, B.; McPhail, S.; Nanson, G.; Pearman, G. I.; Richards, N. G.; Sharkey, T. D.; Temple, R. B.; Weir, B. *Isotopes in tree rings.* 1984. 86 p.

No. 5 Enting, I. G. *Techniques for determining surface sources from surface observations of atmospheric constituents.* 1984. 30 p.

No. 6 Beardsmore, D. J.; Pearman, G. I.; O'Brien, R. C. *The CSIRO (Australia) Atmospheric Carbon Dioxide Monitoring Program: surface data.* 1984. 115 p.

No. 7 Scott, J. C. *High speed magnetic tape interface for a microcomputer.* 1984. 17 p.

No. 8 Galbally, I. E.; Roy, C. R.; Elsworth, C. M.; Rabich, H. A. H. *The measurement of nitrogen oxide (NO, NO_2) exchange over plant/soil surfaces.* 1985. 23 p.

No. 9 Enting, I. G. *A strategy for calibrating atmospheric transport models.* 1985. 25 p.

No. 10 O'Brien, D. M. *TOVPIX: software for extraction and calibration of TOVS data from the high resolution picture transmission from TIROS-N satellites.* 1985. 41 p.

No. 11 Enting, I. G.; Mansbridge, J. V. *Description of a two-dimensional atmospheric transport model.* 1986. 22 p.

No. 12 Everett, J. R.; O'Brien, D. M.; Davis, T. J. *A report on experiments to measure average fibre diameters by optical fourier analysis.* 1986. 22 p.

No. 13 Enting, I. G. *A signal processing approach to analysing background atmospheric constituent data.* 1986. 21 p.

No. 14 Enting, I. G.; Mansbridge, J. V. *Preliminary studies with a two- dimensional model using transport fields derived from a GCM.* 1987. 47 p.

No. 15 O'Brien, D. M.; Mitchell, R. M. *Technical assessment of the joint CSIRO/Bureau of Meteorology proposal for a geostationary imager/sounder over the Australian region.* 1987. 53 p.

No. 16 Galbally, I. E.; Manins, P. C.; Ripari, L.; Bateup, R. *A numerical model of the late (ascending) stage of a nuclear fireball.* 1987. 89 p.

No. 17 Durre, A. M.; Beer, T. *Wind information prediction study: Annaburroo meteorological data analysis.* 1989. 30 p. + diskette.

No. 18 Mansbridge, J. V.; Enting, I. G. *Sensitivity studies in a two-dimensional atmospheric transport model.* 1989. 33 p.

No. 19 O'Brien, D. M.; Mitchell, R. M. *Zones of feasibility for retrieval of surface pressure from observations of absorption in the A band of oxygen.* 1989. 12 p.

No. 20 Evans, J. L. *Envisaged impacts of enhanced greenhouse warming on tropical cyclones in the Australian region.* 1990. 31 p. [Out of print]

No. 21 Whetton, P. H.; Pittock, A. B. *Australian region intercomparison of the results of some general circulation models used in enhanced greenhouse experiments.* 1991. 73 p. [Out of print]

No. 22 Enting, I. G. *Calculating future atmospheric CO_2 concentrations.* 1991. 32 p.

No. 23 Kowalczyk, E. A.; Garratt, J. R.; Krummel, P. B. *A soil-canopy scheme for use in a numerical model of the atmosphere—1D stand-alone model.* 1992. 56 p.

No. 24 Physick, W. L.; Noonan, J. A.; McGregor, J. L.; Hurley, P. J.; Abbs, D. J.; Manins, P. C. *LADM: A Lagrangian Atmospheric Dispersion Model.* 1994. 137 p.

No. 25 Enting, I. G. *Constraining the atmospheric carbon budget: a preliminary assessment.* 1992. 28 p.

No. 26 McGregor, J. L.; Gordon, H. B.; Watterson, I. G.; Dix, M. R.; Rotstayn, L. D. *The CSIRO 9-level atmospheric general circulation model.* 1993. 89 p.

No. 27 Enting, I. G.; Lassey, K. R. *Projections of future CO_2,* with appendix by R.A. Houghton. 1993. 42 p.

No. 28 [Not published]

No. 29 Enting, I. G.; Trudinger, C. M.; Francey, R. J.; Granek, H. *Synthesis inversion of atmospheric CO_2 using the GISS tracer transport model.* 1993. 44 p.

No. 30 O'Brien, D. M. *Radiation fluxes and cloud amounts predicted by the CSIRO nine level GCM and observed by ERBE and ISCCP.* 1993. 37 p.

No. 31 Enting, I. G.; Wigley, T. M. L.; Heimann, M. *Future emissions and concentrations of carbon dioxide: key ocean/atmosphere/land analyses.* 1994. 120 p.

No. 32 Kowalczyk, E. A.; Garratt, J. R.; Krummel, P. B. *Implementation of a soil-canopy scheme into the CSIRO GCM—regional aspects of the model response.* 1994. 59 p.

No. 33 Prata, A. J. *Validation data for land surface temperature determination from satellites.* 1994. 40 p.

No. 34 Dilley, A. C.; Elsum, C. C. *Improved AVHRR data navigation using automated land feature recognition to correct a satellite orbital model.* 1994. 22 p.

No. 35 Hill, R. H.; Long, A. B. *The CSIRO dual-frequency microwave radiometer.* 1995. 16 p.

No. 36 Rayner, P. J.; Law, R. M. *A comparison of modelled responses to prescribed CO_2 sources.* 1995. 84 p.

No. 37 Hennessy, K. J. *CSIRO Climate change output.* 1998. 23 p.

No. 38 Enting, I. G. *Attribution of greenhouse gas emissions, concentrations and radiative forcing.* 1998.